ARTICLES

Synthesis and Magnetic Properties of Single-Crystalline Mn/Fe-Doped and Co-doped ZnS Nanowires and Nanobelts

Taejoon Kang,[†] Joonho Sung,[‡] Wooyoung Shim,[§] Heesung Moon,[||] Jaehun Cho,[⊥] Younghun Jo,[⊥] Wooyoung Lee,[§] and Bongsoo Kim*,[†]

Department of Chemistry, KAIST, Daejeon 305-701, Korea, R&D Center, Dongkuk Steel Mill Company, Ltd., Pohang 790-729, Korea, Department of Materials Science and Engineering, Yonsei University, Seoul 120-749, Korea, Corporate R&D Center, Samsung SDI Company, Ltd., Yong-in 449-577, Korea, and Nano Materials Research Team, KBSI, Daejeon 305-333, Korea

Received: September 23, 2008; Revised Manuscript Received: January 29, 2009

ZnS nanowires and nanobelts doped with Mn and Fe were synthesized by a chemical vapor transport method. The Mn/Fe-doped and co-doped ZnS nanostructures were grown on Au-coated Si substrates. The key to this synthetic process of co-doping lies in the use of metal chloride as a metal carrier. Crystal structure and chemical compositional analyses by transmission electron microscopy (TEM) indicate that the nanowires and nanobelts are single-crystalline and uniformly doped with dopants. Strong emission bands were found from photoluminescence (PL) spectra of Mn/Fe-doped and co-doped ZnS nanowires. The magnetic property measurements from the nanostructure ensemble show that the Curie temperature is above room temperature. The synthesized Mn/Fe-doped and co-doped ZnS nanostructures can be employed in the fabrication of nanoscale magnetic and optical devices.

Introduction

One-dimensional single-crystalline semiconductor nanostructures are emerging as versatile building blocks for nanoscale electronic and photonic devices,[1−4] such as light-emitting diodes (LEDs),[5] field effect transistors (FETs),[6] and electronic sensors,[7] because of their remarkable chemical and physical properties, due to dimensionality and size reduction. ZnS is an important II−VI semiconductor material with a wide band gap of 3.7 eV and has been used as a base material for cathode ray tube (CRT) and field emission display (FED) phosphors, electroluminescent devices, and infrared (IR) windows for a long time.[8−15]

To utilize semiconductor nanostructures as building blocks of functional nanodevices, it is important to synthesize nanostructures that have diverse physical properties. In this regard, many researchers try to synthesize transition-metal-doped semiconductor nanostructures.[3,16−23] Substitutional doping of semiconductors with transition-metal ions can produce magnetic materials called diluted magnetic semiconductors (DMSs).[24] Because DMSs have interesting magnetic properties and can be easily integrated into microelectronic devices, they are considered to be one of the most promising candidate materials for spintronics,[25−27] whose main topic is the manipulation of spin degrees of freedom rather than electric charge in a solid-state system.[28] Recently, many advances have been made in the synthesis of transition-metal-doped III−V and II−VI semiconductor nanostructures as the theoretical work predicted these materials could exhibit high Curie temperatures.[29] The calculations on $Zn_{1-x}X_xS$ nanostructures reported that these materials can be ferromagnetic when X = Cr, Fe, and Ni.[30] Whereas the luminescent properties of various metal-doped ZnS nanoparticles, nanowires, and nanobelts were extensively investigated,[31,32] much less attention has been placed on the magnetic properties of metal-doped ZnS nanostructures of one dimension.

Herein, we report the vapor-phase synthesis of one-dimensional single-crystalline transition-metal-doped ZnS nanowires and nanobelts; the doping elements are Mn, Fe, or (Mn and Fe). We will explain how metal-doped ZnS nanostructures are synthesized, then present the optical and magnetic properties of Mn/Fe-doped and co-doped ZnS nanostructures. These well-defined and composition-tunable ZnS nanostructures would be able to provide new building blocks for various optical and magnetic devices.

Experimental Section

Mn-doped, Fe-doped, and Mn/Fe-co-doped ZnS nanostructures were synthesized in a conventional horizontal furnace system with a 1 in. diameter quartz tube. For the synthesis of Mn-doped ZnS nanowires, a mixture of ZnO powder (0.30 g, 99.99%, Sigma-Aldrich), MnS powder (0.33 g, 99.9%, Sigma-Aldrich), and $MnCl_2$ beads (0.10 g, 99.999%, Sigma-Aldrich) was placed in an alumina boat in the middle of the heating zone. The molar ratio of the three reagents was about 5:5:1. The temperature of the furnace was raised to 950 °C and maintained at this temperature for 20 min. The precursor vapor was carried by the flow of 500 sccm of argon gas at a pressure of 5 Torr to a Au-coated Si substrate, where white product was produced.

* To whom correspondence should be addressed. Fax: +82-42-350-2810. E-mail: bongsoo@kaist.ac.kr.
[†] KAIST.
[‡] Dongkuk Steel Mill Company, Ltd.
[§] Yonsei University.
[||] Samsung SDI Company, Ltd.
[⊥] KBSI.

10.1021/jp808433b CCC: $40.75
Published on Web 03/17/2009

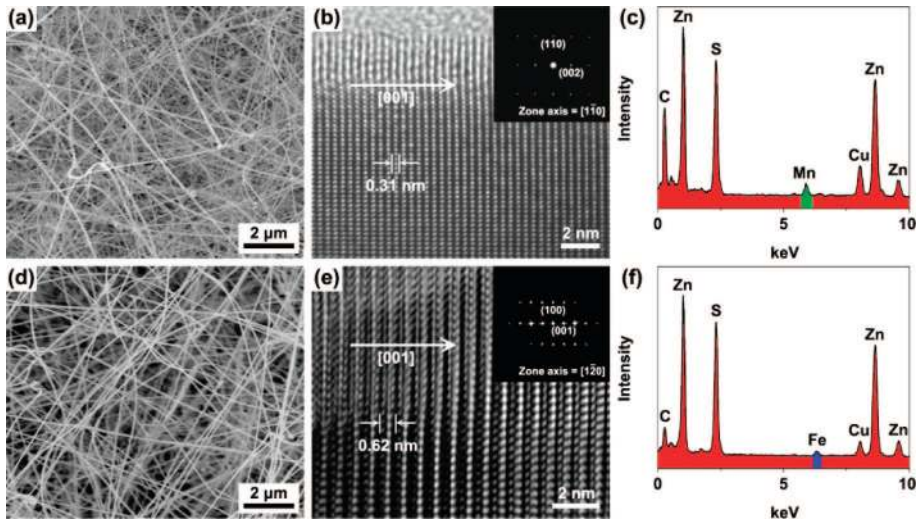

Figure 1. SEM images of (a) Mn-doped and (d) Fe-doped ZnS nanowires grown on Au-coated Si substrates. HRTEM images and corresponding EDS spectra of (b,c) Mn-doped and (e,f) Fe-doped ZnS nanowires. The insets in the HRTEM images are (b) SAED pattern and (e) two-dimensional FFT.

Fe-doped ZnS nanowires were synthesized by a similar method, except that FeS powder (0.33 g, 99.9%, Sigma-Aldrich) and $FeCl_2$ beads (0.10 g, 99.998%, Sigma-Aldrich) were used instead of MnS and $MnCl_2$.

To synthesize Mn/Fe-co-doped ZnS nanowires and nanobelts, ZnO powder (0.30 g), FeS powder (0.33 g), and $MnCl_2$ beads (0.10 g) were used. The reagents were mixed together and then put in an alumina boat, which was inserted into a quartz tube and heated to 950 °C under a constant argon flow of 500 sccm. The nanowires were grown at a total pressure of 5 Torr, whereas nanobelts were synthesized at 20 Torr. After the furnace was cooled to room temperature, the Au-coated Si substrate became covered by a white material.

The scanning electron microscope (SEM) images of the nanostructures were taken on a Phillips XL30S operated at 10 kV. For TEM investigation, as-grown nanowires and nanobelts were dispersed in ethanol and a drop of solution was put on a holey carbon-coated copper grid. High-resolution transmission electron microscope (HRTEM) images and selected-area electron diffraction (SAED) patterns were taken on a JEOL JEM-2100F microscope operated at 200 kV. Chemical compositions of the nanostructures were studied by energy-dispersive X-ray spectroscopy (EDS) attached to the TEM. The X-ray diffraction (XRD) patterns of nanowires and nanobelts were recorded using a Rigaku D/max-RC (12 kW) diffractometer with the Cu Kα radiation ($\lambda = 0.15406$ nm). Room-temperature PL spectra were obtained at an excitation wavelength of 266 nm. Magnetic properties of the Mn/Fe-doped and co-doped ZnS nanostructures were studied using a superconducting quantum interference device (SQUID) magnetometer.

Results and Discussion

Typical SEM images of Mn-doped and Fe-doped ZnS nanowires are shown in Figure 1a,d. The as-grown nanowires were produced in high density and uniformly covered the entire Si substrate. The nanowires are tens of micrometers long and 70−100 nm in diameter. The micrographs clearly show the nanowires with a clean and smooth surface, whereas no secondary phases or extra structural features are observed. To characterize the crystal structure, growth direction, and elemental composition of nanowires, we carried out HRTEM, SAED, and EDS studies. The HRTEM image of the Mn-doped ZnS nanowire shows clear lattice fringes, which confirm the single-crystalline nature of the nanowire (Figure 1b). The lattice spacing of 0.31 nm, consistent with the (002) crystal plane of a wurtzite ZnS structure, indicates that the nanowire grew in the [001] direction, as marked with a white arrow. The inset is a SAED pattern that was observed at the [1−10] zone axis. All of the spot patterns are completely assigned to a wurtzite ZnS structure. The EDS spectrum of a Mn-doped ZnS nanowire indicates that Zn and S are major elements, with about 3% Mn (Figure 1c). The composition is uniform throughout the nanowire, according to the EDS mapping. Lines due to Cu and C are from the TEM grid. EDS spectra from other nanowires are similar, and the Mn content is not much varied.

The HRTEM image of an Fe-doped ZnS nanowire shows clear lattice fringes of the (001) crystal plane, indicating again the growth direction is [001] (Figure 1c). The two-dimensional FFT of the lattice-resolved image obtained from the HRTEM can also be indexed to the wurtzite ZnS structure. The crystal structure and growth direction of an Fe-doped ZnS nanowire are the same as a Mn-doped one. The EDS spectrum in Figure 1f also shows that the nanowire is composed of Zn, S, and Fe only. The atomic percent of Fe dopant is about 2%.

The single-metal-doped ZnS nanowires were synthesized by precursors of ZnO, MS, and MCl_2 (M = Mn or Fe). By increasing the reaction temperature, MCl_2 is vaporized first because of its lower melting point ($MnCl_2$, 654 °C; $FeCl_2$, 674 °C), compared to that of other precursors (ZnO, 1975 °C; MnS, 1610 °C; FeS, 1188 °C). When the temperature rises higher, MCl_2 decomposes into M and Cl_2. Various nanowires were synthesized by modifying this reaction.[33,34] The decomposition of MCl_2 and growth of ZnS nanowires occur simultaneously; thus, the Mn or Fe atoms were uniformly doped into ZnS crystals, and decomposed Cl_2 gas was passed through the quartz tube. The final products on Si substrates are Mn- or Fe-doped ZnS nanowires, which have no secondary phase. The formation of metal-doped ZnS nanowires can be explained by the following plausible reaction pathway:

In this reaction, ZnO plays a role as a Zn source and desulfurization reagent for MS and MS becomes both a stable S source and a reducing agent of ZnO. Since oxygen is more reactive than sulfur at high temperatures, ZnS can be easily oxidized into ZnO at high temperatures, with only traces of O_2

$$\mathrm{ZnO\ (powder) + MS\ (powder) + MCl_2\ (beads)} \leftrightarrow \mathrm{Zn_{1-x}M_xS\ (nanowires) + Cl_2\ (gas) + M_3O_4\ (residues\ in\ the\ boat)\ (M = Mn\ or\ Fe)}$$

gas.[35] Yuan et al. reported that ZnO nanowires were grown by thermal evaporation of ZnS powder in a vacuum chamber under a flow of 200 sccm of argon gas because some oxygen can leak into the reaction chamber.[36] Thus, graphite powder was used to maintain a reductive atmosphere for the synthesis of ZnS nanostructures starting with ZnS powder.[11,37] Herein, we used ZnO and MS powders for the synthesis of ZnS nanostructures. The metal atoms decomposed from the MS precursor prevent oxidation of ZnS nanowires by reacting with O_2 to produce metal oxides. Paramagnetic metal oxide clusters (Fe_3O_4 or Mn_3O_4) were found in the alumina boat after the reaction. Therefore, as-synthesized ZnS nanowires were not oxidized under a flow of argon when ZnO and MS are used as precursors. Moreover, Hussain et al. reported that ZnS is not fully oxidized when ZnO and FeS reacted under an atmospheric condition.[38] It is likely that using ZnO as a reactant suppresses the conversion of as-synthesized ZnS into ZnO.

For the formation of the metal-doped ZnS phase, the presence of MCl_2, mixed with other precursors, is critical because MCl_2 plays a role as a carrier of doping metals. Pure ZnS nanowires were synthesized when only ZnO and MS were used as precursors.[39] Metal chlorides have been employed for the synthesis of nanostructures, such as Mn-doped ZnS[31] and Cu-doped GaN.[20] Similarly, Choi et al. reported that the Mn-doped GaN nanowires were grown by transporting the $GaCl_3$ and $MnCl_2$ produced by the reaction of metallic Ga and Mn with HCl gas.[16,40] In the present experiment, the reaction of ZnO and MS is employed to synthesize the ZnS nanowires at 900−950 °C, which is lower than the temperature of thermal evaporation techniques using ZnS powder (1150 °C). The lower reaction temperature is more advantageous for doping ZnS nanostructures by MCl_2. Because MCl_2 vaporizes at ~600 °C, it is much more convenient to use the reaction temperature of 900 °C rather than 1150 °C for successful control of the reaction condition.

By employing a mixture of ZnO, FeS, and $MnCl_2$, the Mn/Fe-co-doped ZnS nanowires were synthesized. The SEM image of as-grown nanowires is shown in Figure 2a. The length and diameter of the nanowires are the same as those of single-metal-doped nanowires. Figure 2b is a HRTEM image and two-dimensional FFT obtained from the HRTEM result (inset). The Mn/Fe-co-doped ZnS nanowires are single-crystalline and grown in the [001] direction. The 0.62 nm of lattice spacing is clearly observed in a HRTEM image, and the representative two-dimensional FFT spots are indexed to the wurtzite ZnS structure. The EDS line scan result (Figure 2c) and spectrum (Figure 2d) of a Mn/Fe-co-doped ZnS nanowire confirm the uniform doping of Mn and Fe. The composition of Mn and Fe is about 1 and 2%, respectively.

In this synthetic method, $MnCl_2$ plays a role as a Mn-carrying agent. Furthermore, by the reaction with FeS or Fe, it generates $FeCl_2$ that becomes an Fe-carrying agent. Thus, the co-doping of Mn and Fe becomes possible. Yu et al. synthesized Fe/Co-co-doped ZnO nanowires by using the mixture of Zn, Fe, and $CoCl_2$,[19] and Park et al. reported Mn/Zn-co-doped CdS nanowires by using CdS, ZnS, and $MnCl_2$.[21] After further optimization, this synthetic process would be able to contribute to the synthesis of various metal-co-doped ZnS nanostructures by using diverse metal-containing compounds.

A typical SEM image of Mn/Fe-co-doped ZnS nanobelts is illustrated in Figure 3a. The micrograph of the as-synthesized

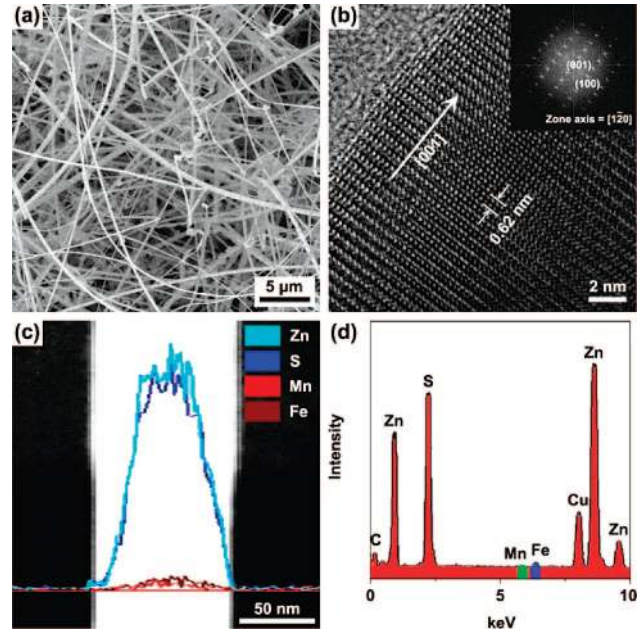

Figure 2. (a) SEM image of Mn/Fe-co-doped ZnS nanowires. (b) HRTEM image of a nanowire in (a). The inset shows the two-dimensional FFT from the HRTEM image. (c,d) EDS line profiles and spectrum for Mn/Fe-co-doped ZnS nanowire.

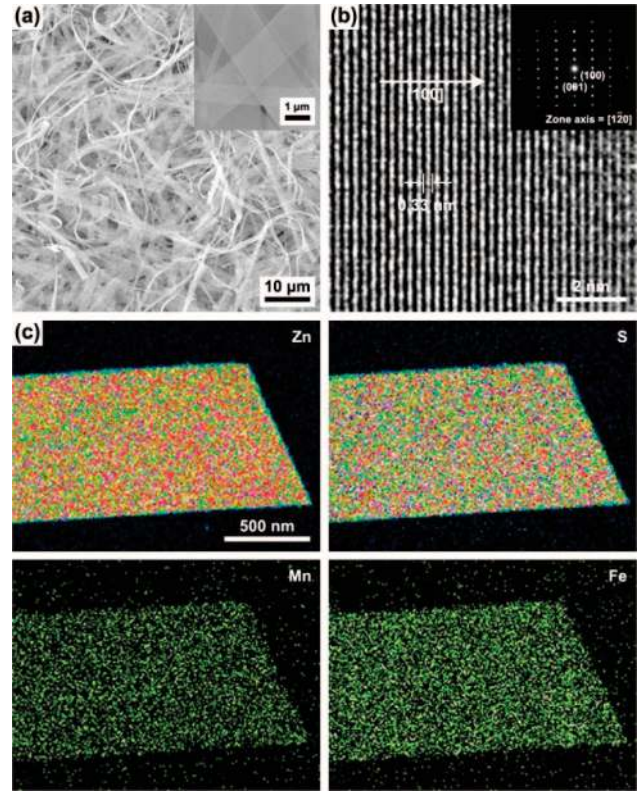

Figure 3. (a) SEM image of Mn/Fe-co-doped ZnS nanobelts. The inset is a magnified SEM image of nanobelts. (b) HRTEM image of a nanobelt in (a). The inset is an SAED pattern. (c) EDS mapping profiles for the nanobelt with Zn, S, Mn, and Fe.

nanobelts shows that uniform nanostructures were formed in high density. The nanobelts are several tens of micrometers long and several hundreds of nanometers wide. The inset image shows that Mn/Fe-co-doped ZnS nanobelts are electron-transparent, indicating that the nanobelts are very thin. The crystal structure and chemical composition of a single Mn/Fe-co-doped ZnS nanobelt were analyzed by TEM. Figure 3b shows

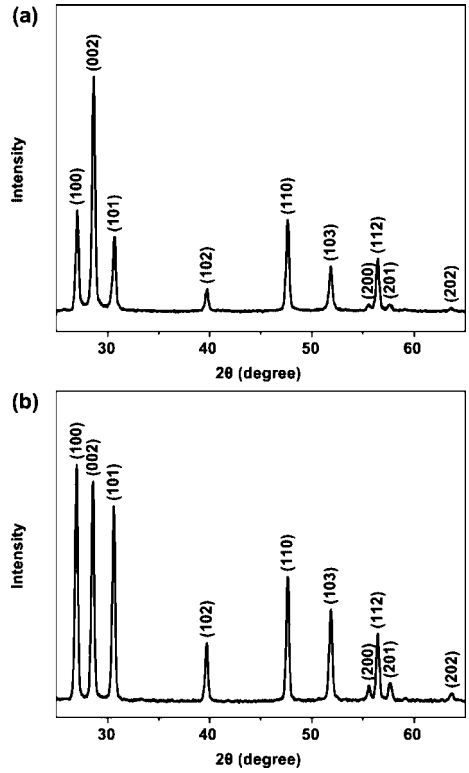

Figure 4. XRD patterns of Mn/Fe-co-doped ZnS (a) nanowires and (b) nanobelts, both with wurtzite structures.

the HRTEM image of a nanobelt in Figure 3a, and the inset is a corresponding SAED pattern. Different than those of nanowires, the HRTEM image shows distinct lattice fringes along the direction of [100] and the SAED pattern also reveals that the nanobelts have a single-crystalline wurtzite structure grown along the [100] direction. The zone axis of the SAED pattern is a [1−20] crystal plane. Elemental mapping profiles of a Mn/Fe-co-doped ZnS nanobelt for Zn, S, Mn, and Fe are presented in Figure 3c. These pictures, showing the distinct shape of a nanobelt without any partial aggregation, indicate homogeneous distribution of Mn and Fe in the nanobelt. The atomic compositions of Mn and Fe are 1 and 2%, respectively, similar to those of the nanowires. This synthetic method provides single-crystalline Mn/Fe-doped and co-doped ZnS nanowires and nanobelts with no phase separation or grain boundaries, which have been problems because they can induce the ferromagnetism of the DMSs to arise from magnetic secondary clusters.[20]

XRD patterns of Mn/Fe-co-doped ZnS nanowires and nanobelts are shown in Figure 4. All of the diffraction peaks are perfectly indexed to wurtzite ZnS structures (JCPDS 36-1450), revealing that the doping of Mn and Fe does not change the crystal structure. Other peaks due to Mn- or Fe-related impurities were not detected. Different peak intensities indicate that the growth directions of nanobelts and nanowires are different, as explained previously.

The Mn/Fe-co-doped ZnS nanowires and nanobelts were synthesized on Au-coated Si substrates through a simple chemical vapor transport method based on a vapor−liquid−solid (VLS) mechanism.[2] The Zn, S, and small amount of Mn and Fe form an alloy with the Au. When the concentration of precursors is higher than the saturation threshold, the ZnS compound precipitates in a wurtzite structure with a preferential growth orientation. In this experiment, the nanobelts grow when the total pressure is higher (20 Torr) and the nanowires at the lower total pressure (5 Torr). This morphology change can be

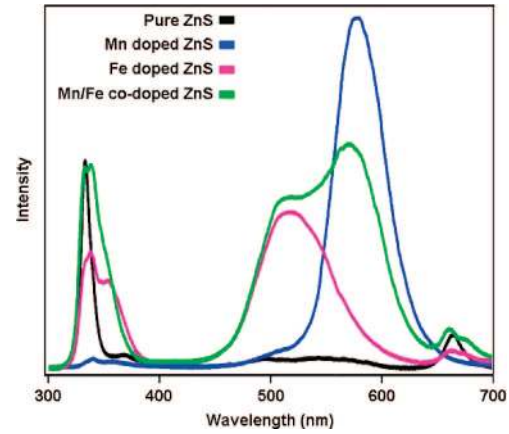

Figure 5. PL spectra of pure, Mn/Fe-doped, and co-doped ZnS nanowires at room temperature.

ascribed to the change in the degree of supersaturation, depending on the total pressure. The supersaturation is determined by the vapor pressure of the growing materials and the temperature of the substrate.[41] Because the temperature of the substrate was the same, the morphology of the nanostructures was determined mainly by the vapor pressure of the growing materials. When the total pressure increases by reducing the pumping speed, the vapor pressure of the growing materials is also increased and, thus, nanobelts are the preferred product of the synthesis. This observation is in accordance with the previous results for one-dimensional nanostructure synthesis, in which a higher degree of supersaturation favors the growth of nanobelts, whereas nanowires are favored at a lower degree of supersaturation.[42,43] Moreover, we find that the growth directions of nanowires and nanobelts are different. This is also associated with the change of synthesis conditions. Thermodynamically, the fastest growth direction for a wurtzite structure is [001]. By altering the synthesis conditions, however, growth rates of crystalline planes can be changed[44] and, thus, ZnS nanostructures with various growth directions could be synthesized.[45−49] In this experiment, we synthesized Mn/Fe-doped and co-doped ZnS nanowires and nanobelts with different growth directions by changing the total pressure condition.

PL studies of Mn/Fe-doped and co-doped ZnS nanowires were carried out by using a 266 nm excitation source. Figure 5 shows strong emission bands in the UV−vis range. From the PL spectrum of pure ZnS nanowires (black spectrum), only a band-edge emission near 335 nm was observed clearly.[39] This implies that as-grown ZnS nanowires are of high quality and contain few defects. The PL properties of Mn-doped ZnS nanostructures had been extensively studied. The transfer of electrons and holes into the electronic level of the Mn ions induces the characteristic emission band around 580 nm, which is associated with the $^4T_1 \rightarrow {}^6A_1$ transition in Mn^{2+}.[31] Hence, the emission band around 580 nm for Mn-doped ZnS nanowires (blue spectrum) is attributed to Mn^{2+} impurities. For Fe-doped ZnS NWs (magenta spectrum), a 520 nm emission band was observed. In some of the literature, a green emission band was found from Au catalytically grown ZnS nanowires because of Au impurities[49,50] and there was no visible emission band arising from Fe doping.[51] In the present experiment, all ZnS nanowires were synthesized by using Au catalyst. However, the 520 nm band was observed only for Fe-doped and Mn/Fe-co-doped ZnS nanowires. The PL spectra of pure and Mn-doped ZnS nanowires did not show the 520 nm band. Thus, we interpret that the broad emission band around 520 nm is associated with Fe doping, and further study is needed to understand the detailed

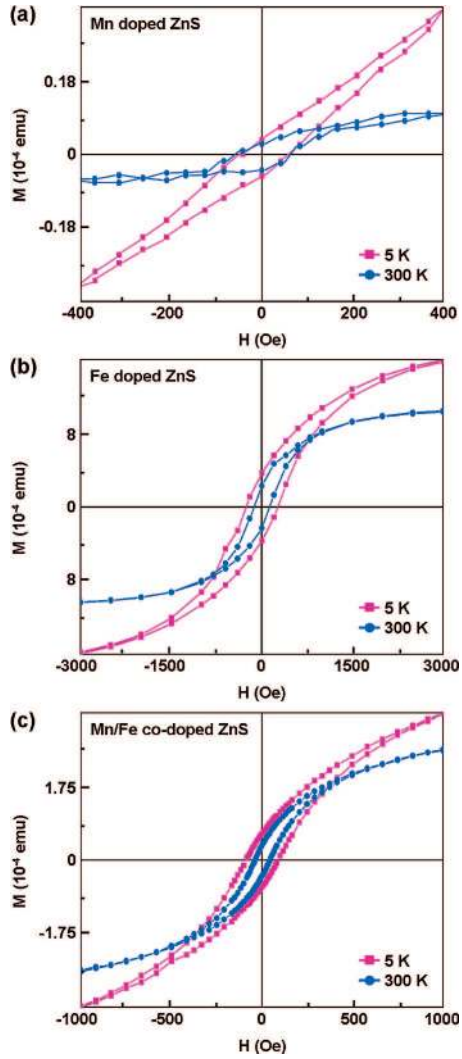

Figure 6. Magnetization loops measured at 5 and 300 K of (a) Mn-doped, (b) Fe-doped, and (c) Mn/Fe-co-doped ZnS nanostructures. Hysteresis behaviors are observed at 5 and 300 K.

origin of this emission band. The PL spectrum of Mn/Fe-co-doped ZnS nanowires (green spectrum) shows two bands around 520 and 580 nm, as expected from the results of Mn-doped and Fe-doped ZnS nanowires.

The magnetic properties of the Mn/Fe-doped and co-doped ZnS nanostructures were investigated by a SQUID magnetometer. The magnetization versus an applied magnetic field measured at 5 and 300 K is shown in Figure 6. The diamagnetic characteristic of a Si substrate is subtracted. The magnetic hysteresis loops are clearly seen at both temperatures, indicating that these ZnS nanostructures are ferromagnetic at room temperature. Since the mass of ZnS nanostructures is not exactly known, the magnetization value was not directly compared. Nevertheless, Fe-doped ZnS nanowires exhibit the largest magnetization value ($H_c \sim 130$ Oe).

The origin of the ferromagnetism of magnetic-element-doped semiconductors is still controversial, due to the possibility of magnetic secondary phases and the uncertainty of magnetic interactions. In our experiment, careful analyses of Mn/Fe-doped and co-doped ZnS nanostructures were performed by using SEM, HRTEM, and XRD patterns. There is no evidence of magnetic clusters or secondary phases in Mn/Fe-co-doped ZnS nanostructures. This synthetic success provides new DMS nanostructured materials with a Curie temperature above room temperature. The as-grown nanostructures can be employed to fabricate nanoscale magnetic devices.

Conclusion

We successfully synthesized Mn-doped, Fe-doped, and Mn/Fe-co-doped ZnS nanostructures by using a chemical vapor transport method. The metal chlorides play a critical role in the substitution of the Zn with dopants. The elemental composition analyses show direct evidence of homogeneous doping in ZnS nanostructures. The room-temperature PL spectra of Mn/Fe-doped and co-doped ZnS nanowires reveal strong emission bands in the UV−vis range, and the magnetic measurements present that the as-synthesized Mn/Fe-doped and co-doped ZnS nanostructures have room-temperature ferromagnetism. These results show that the one-dimensional metal-doped ZnS nanostructures can be applied to magnetic and optical nanodevices.

Acknowledgment. This research was supported by KOSEF through NRL (ROA-2007-000-20127-0), and the Center for Nanostructured Materials Technology under "21st Century Frontier R&D Programs" of the MOST, Korea (08K1501-02210). PL analysis was performed at the Korea Basic Science Institute in Gwangju.

References and Notes

(1) Hu, J.; Odom, T. W.; Lieber, C. M. *Acc. Chem. Res.* **1999**, *32*, 435.
(2) Xia, Y.; Yang, P.; Sun, Y.; Wu, Y.; Mayers, B.; Gates, B.; Yin, Y.; Kim, F.; Yan, H. *Adv. Mater.* **2003**, *15*, 353.
(3) Radovanovic, P. V.; Barrelet, C. J.; Gradecak, S.; Qian, F.; Lieber, C. M. *Nano Lett.* **2005**, *5*, 1407.
(4) Ma, D. D. D.; Lee, S.-T.; Mueller, P.; Alvarado, S. F. *Nano Lett.* **2006**, *6*, 926.
(5) Zhong, Z.; Qian, F.; Wang, D.; Lieber, C. M. *Nano Lett.* **2003**, *3*, 343.
(6) Zhong, Z.; Wang, D.; Cui, Y.; Bockrath, M. W.; Lieber, C. M. *Science* **2003**, *302*, 1377.
(7) Cui, Y.; Wei, Q.; Park, H.; Lieber, C. M. *Science* **2001**, *293*, 1289.
(8) Jiang, Y.; Meng, X.-M.; Liu, J.; Xie, Z.-Y.; Lee, C.-S.; Lee, S.-T. *Adv. Mater.* **2003**, *15*, 323.
(9) Yin, L.-W.; Bando, Y.; Zhan, J.-H.; Li, M.-S.; Golberg, D. *Adv. Mater.* **2005**, *17*, 1972.
(10) Moore., D.; Wang, Z. L. *J. Mater. Chem.* **2006**, *16*, 3898.
(11) Fang, X.; Bando, Y.; Golberg, D. *J. Mater. Sci. Technol.* **2008**, *24*, 512.
(12) Fang, X.; Bando, Y.; Ye, C.; Shen, G.; Golberg, D. *J. Phys. Chem. C* **2007**, *111*, 8469.
(13) Chai, L.; Du, J.; Xiong, S.; Li, H.; Zhu, Y.; Qian, Y. *J. Phys. Chem. C* **2007**, *111*, 12658.
(14) Fang, X.-S.; Ye, C.-H.; Zhang, L.-D.; Wang, Y.-H.; Wu, Y.-C. *Adv. Funct. Mater.* **2005**, *15*, 63.
(15) Hongliang, G.; Min, Z.; Hua, L.; Qiong, W.; Pingzhan, S. *Rare Met. Mater. Eng.* **2008**, *37*, 261.
(16) Choi, H.-J.; Seong, H.-K.; Chang, J.; Lee, K.-I.; Park, Y.-J.; Kim, J.-J.; Lee, S.-K.; He, R.; Kuykendall, T.; Yang, P. *Adv. Mater.* **2005**, *17*, 1351.
(17) Biswas, S.; Kar, S.; Chaudhuri, C. *J. Phys. Chem. B* **2005**, *109*, 17526.
(18) Na, C. W.; Han, D. S.; Kim, D. S.; Kang, Y. J.; Lee, J. Y.; Park, J.; Oh, D. K.; Kim, K. S.; Kim, D. *J. Phys. Chem. B* **2006**, *110*, 6699.
(19) Liu, L. Q.; Xiang, B.; Zhang, X. Z.; Zhang, Y.; Yu, D. P. *Appl. Phys. Lett.* **2006**, *88*, 063104.
(20) Seong, H.-K.; Kim, J.-Y.; Kim, J.-J.; Lee, S.-C.; Kim, S.-R.; Kim, U.; Park, T.-E.; Choi, H.-J. *Nano Lett.* **2007**, *7*, 3366.
(21) Kim, D. S.; Cho, Y. J.; Park, J.; Yoon, J.; Jo, Y.; Jung, M.-H. *J. Phys. Chem. C* **2007**, *111*, 10861.
(22) Kar, S.; Biswas, S. *J. Phys. Chem. C* **2008**, *112*, 11144.
(23) Yatsunenko, S.; Świætek, K.; Godlewski, M.; Fröba, M.; Klar, P. J.; Heimbrodt, W. *Opt. Mater.* **2008**, *30*, 753.
(24) Furdyna, J. K., Kossut, J., Eds. *Diluted Magnetic Semiconductors*; Academic Press: New York, 1988; Vol. 25.
(25) Ohno, H. *Science* **1998**, *281*, 951.
(26) Malajovich, I.; Berry, J. J.; Samarth, N.; Awshalom, D. D. *Nature* **2001**, *411*, 770.

(27) Wolf, S. A.; Awschalom, D. D.; Buhrman, R. A.; Daughton, J. M.; von Molnar, S.; Roukes, M. L.; Chtchelkanova, A. Y.; Treger, D. M. *Science* **2001**, *294*, 1488.
(28) Zutic, I.; Fabian, J.; Sarma, S. D. *Rev. Mod. Phys.* **2004**, *76*, 323.
(29) Dietl, T.; Ohno, H.; Matsukura, F.; Cibert, J.; Ferrand, D. *Science* **2000**, *287*, 1019.
(30) Stern, R. A.; Schuler, T. M.; MacLaren, J. M.; Ederer, D. L.; Perez-Dieste, V.; Himpsel, F. J. *J. Appl. Phys.* **2004**, *95*, 7468.
(31) Liu, J. Z.; Yan, P. X.; Yue, G. H.; Chang, J. B.; Qu, D. M.; Zhuo, R. F. *J. Phys. D: Appl. Phys.* **2006**, *39*, 2352.
(32) Bhattacharya, S.; Chakravorty, D. *Chem. Phys. Lett.* **2007**, *444*, 319.
(33) Seo, K.; Varadwaj, K. S. K.; Mohanty, P.; Lee, S.; Jo., Y.; J., M.-H.; Kim, J.; Kim, B. *Nano Lett.* **2007**, *7*, 1240.
(34) Varadwaj, K. S. K.; Seo, K.; In, J.; Mohanty, P.; Park, J.; Kim, B. *J. Am. Chem. Soc.* **2007**, *129*, 8594.
(35) Ge, J.-P.; Wang, J.; Zhang, H.-X.; Wang, X.; Peng, Q.; Li, Y.-D. *Adv. Funct. Mater.* **2005**, *15*, 303.
(36) Yuan, H. J.; Xie, S. S.; Liu, D. F.; Yan, X. Q.; Zhou, Z. P.; Ci, L. J.; Wang, J. X.; Gao, Y.; Song, L.; Liu, L. F.; Zhou, W. Y.; Wang, G. *Chem. Phys. Lett.* **2003**, *371*, 337.
(37) Zhu, Y.-C.; Bando, Y.; Xue, D.-F. *Appl. Phys. Lett.* **2003**, *82*, 1769.
(38) Hussain, S. G.; Liu, D.; Huang, X.; Sulieman, K. M.; Liu, J.; Liu, H.; Rasool, R. U. *J. Phys. D: Appl. Phys.* **2007**, *40*, 7662.
(39) Moon, H.; Nam, C.; Kim, C.; Kim, B. *Mater. Res. Bull.* **2006**, *41*, 2013.
(40) Oh, E.; Choi, J. H.; Seong, H.-K.; Choi, H.-J. *Appl. Phys. Lett.* **2006**, *89*, 092109.
(41) Seo, K.; Varadwaj, K. S. K.; Cha, D.; In, J.; Kim, J.; Park, J.; Kim, B. *J. Phys. Chem. C* **2007**, *111*, 9072.
(42) Liang, C.; Shimizu, Y.; Sasaki, T.; Umehara, H.; Koshizaki, N. *J. Phys. Chem. B* **2004**, *108*, 9728.
(43) Dai, Z. R.; Pan, Z. W.; Wang, Z. L. *Adv. Funct. Mater.* **2003**, *13*, 9.
(44) Ma., C.; Moore, D.; Ding, Y.; Li, J.; Wang, Z. L. *Int. J. Nanotechnol.* **2004**, *1*, 431.
(45) Yuan, H. J.; Xie, S. S.; Liu, D. F.; Yan, X. Q.; Zhou, Z. P.; Ci, L. J.; Wang, J. X.; Gao, Y.; Song, L.; Liu, L. F.; Zhou, W. Y.; Wang, Z. G. *J. Cryst. Growth* **2003**, *258*, 225.
(46) Moore., D. F.; Ding, Y.; Wang, Z. L. *J. Am. Chem. Soc.* **2004**, *126*, 14372.
(47) Kar, S.; Chaudhuri, S. *J. Phys. Chem. B* **2005**, *109*, 3298.
(48) Biswas, S.; Ghoshal, T.; Kar, S.; Chakrabarti, S.; Chaudhuri, S. *Cryst. Growth Des.* **2008**, *8*, 2171.
(49) Wang, Y.; Zhang, L.; Liang, C.; Wang, G.; Peng, X. *Chem. Phys. Lett.* **2002**, *357*, 314.
(50) Zhang, Z.; Wang, J.; Yuan, H.; Gao, Y.; Liu, D.; Song, L.; Xiang, Y.; Zhao, X.; Liu, L.; Luo, S.; Dou, X.; Mou, S.; Zhou, W.; Xie, S. *J. Phys. Chem. B* **2005**, *109*, 18352.
(51) Godlewski, M.; Skowronski, M. *Phys. Rev. B* **1985**, *32*, 4007.

JP808433B